



# Ewing's sarcoma precursors are highly enriched in embryonic osteochondrogenic progenitors

Miwa Tanaka,<sup>1</sup> Yukari Yamazaki,<sup>1</sup> Yohei Kanno,<sup>1</sup> Katsuhide Igarashi,<sup>2</sup> Ken-ichi Aisaki,<sup>2</sup> Jun Kanno,<sup>2</sup> and Takuro Nakamura<sup>1</sup>

<sup>1</sup>Division of Carcinogenesis, The Cancer Institute, Japanese Foundation for Cancer Research, Tokyo, Japan.

<sup>2</sup>Division of Cellular and Molecular Toxicology, Biosafety Research Center, National Institute of Health Science, Tokyo, Japan.

**Ewing's sarcoma is a highly malignant bone tumor found in children and adolescents, and the origin of this malignancy is not well understood. Here, we introduced a Ewing's sarcoma-associated genetic fusion of the genes encoding the RNA-binding protein EWS and the transcription factor ETS (*EWS-ETS*) into a fraction of cells enriched for osteochondrogenic progenitors derived from the embryonic superficial zone (eSZ) of long bones collected from late gestational murine embryos. *EWS-ETS* fusions efficiently induced Ewing's sarcoma-like small round cell sarcoma formation by these cells. Analysis of the eSZ revealed a fraction of a precursor cells that express growth/differentiation factor 5 (*Gdfs*), the transcription factor *Erg*, and parathyroid hormone-like hormone (*Pthlh*), and selection of the *Pthlh*-positive fraction alone further enhanced *EWS-ETS*-dependent tumor induction. Genes downstream of the *EWS-ETS* fusion protein were quite transcriptionally active in eSZ cells, especially in regions in which the chromatin structure of the ETS-responsive locus was open. Inhibition of  $\beta$ -catenin, poly (ADP-ribose) polymerase 1 (PARP1), or enhancer of zeste homolog 2 (*EZH2*) suppressed cell growth in a murine model of Ewing's sarcoma, suggesting the utility of the current system as a preclinical model. These results indicate that eSZ cells are highly enriched in precursors to Ewing's sarcoma and provide clues to the histogenesis of Ewing's sarcoma in bone.**

## Introduction

Ewing's sarcoma is a highly malignant bone tumor in children and adolescents. It frequently develops as a small round cell sarcoma in the metaphysis of long bones (1). The origin of Ewing's sarcoma has been an enigma since the first case was reported in 1921 (2). Primitive neural crest cells, hematopoietic cells, and muscle cells as well as mesenchymal stem cells (MSCs) have been considered possible cells of origin (3, 4). Chromosomal translocation-related genetic fusions between *EWSR1* on chromosome 22 and genes encoding ETS family transcription factors, such as *FLI1* and *ERG*, were then identified. The *EWS* and the transcription factor ETS (*EWS-ETS*) fusion is now considered a genetic hallmark of human Ewing's sarcoma (5–7). However, it has been difficult to establish an appropriate animal model by introduction of *EWS-ETS* chimeras (8), suggesting that introduction of *EWS-ETS* is not sufficient to define the origin of the tumors. A few groups have reported successful development of Ewing's sarcoma-like tumors by introduction of *EWS-FLI1* into murine mesenchymal cells (9, 10). However, it is unclear whether there is a special subfraction that includes the cell of origin of Ewing's sarcoma. The difficulty of inducing Ewing's sarcoma suggests that the target cells of *EWS-ETS* might be the cells of a narrow lineage and/or of a limited differentiation stage.

Unlike osteosarcoma, which generally involves the metaphyses of long tubular bones, Ewing's sarcoma occurs at almost equal frequencies in flat bones and the diaphysis of tubular bones (11). This fact suggests that mutations related to the proliferation of bony tissue might not contribute to the genesis of Ewing's sarcoma. Moreover, it suggests that the primary genetic event, the *EWS-ETS* fusion, might occur at an earlier stage of bone development.

Members of the *ETS* family of genes that are involved in *EWS* fusions are important for transcriptional regulation in mouse embryonic and perinatal limb skeletogenesis (12). Accumulation of *Erg*<sup>+</sup> progenitor cells occurs in the embryonic superficial zone (eSZ) of long bones from dpc 15.5 to P7, after which expression is downregulated rapidly (13, 14). These results suggest that temporospatial expression of *Erg* might be critical for induction of bipotential progenitors during osteochondrogenic differentiation and that dysregulated expression due to chromosomal translocation and fusion to *EWSR1* might result in abnormal accumulation of progenitor cells that exhibit increased proliferative potency (10).

To clarify the possible cellular origin of Ewing's sarcoma, we purified eSZ cells from murine embryonic long bones that expressed *Erg* and introduced *EWS-FLI1* or *EWS-ERG* fusion genes. We found that *EWS-ETS* target cells were highly enriched in the eSZ fraction. Moreover, the epigenetic status of genes responsive to transcriptional regulation by *EWS-ETS* is important for Ewing's sarcoma development and its phenotypic manifestation.

## Results

**Development of Ewing's sarcoma-like small round cell tumors by *EWS-ETS* expression in the eSZ cells.** *Erg*, one of the *EWS* fusion partners in Ewing's sarcoma, is transiently expressed in the joint surface of embryonic and perinatal bones. Therefore, we predicted that the *EWS-ETS* fusion would affect differentiation and induce abnormal proliferation of *Erg*-expressing cells. To test this hypothesis, femoral and humeral bones of dpc 18.5 murine embryos were separated into the eSZ, embryonic growth plate (eGP), the embryonic shaft and synovial regions (eSyR) by microdissection (Figure 1A). Embryonic mesenchymal cells of the head and trunk were also prepared. Each cell fraction was mildly digested with type I collagenase. The cells were immediately subjected to retrovirus-mediated

**Conflict of interest:** The authors have declared that no conflict of interest exists.

**Citation for this article:** *J Clin Invest.* 2014;124(7):3061–3074. doi:10.1172/JCI12399.

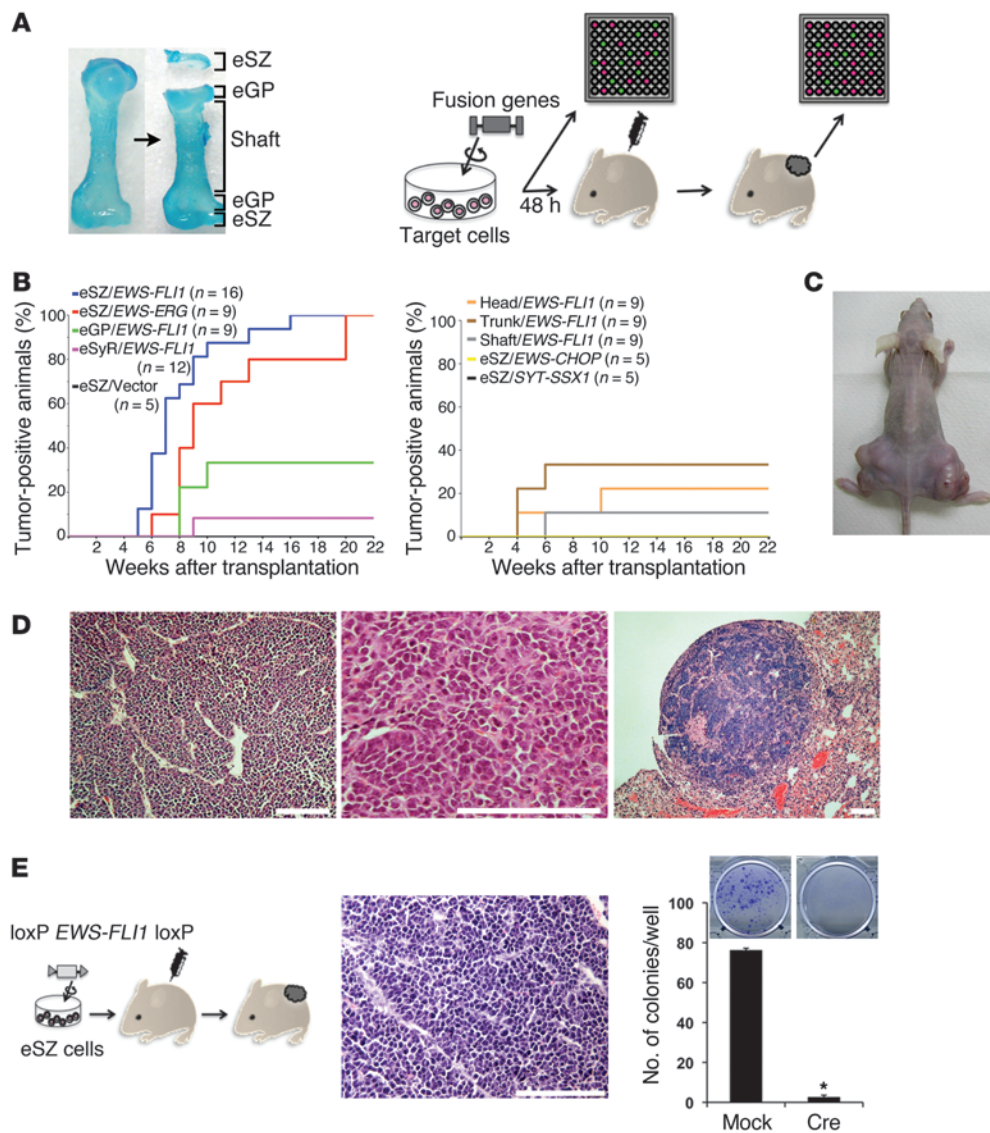


**Figure 1**

Development of murine Ewing's sarcoma. (A) Microdissection of mouse embryonic bone. The femur was lightly stained with methylene blue. Experimental strategy of the ex vivo model. Each cell type targeted with *EWS-ETS* was injected into nude mice or subjected to gene expression profiling. (B) Cumulative incidence (percentage) of small round cell tumors induced by eSZ, eGP, and eSyR cells expressing *EWS-ETS* or by eSZ with an empty vector and by embryonic mesenchymal cells of the trunk, head, and shaft expressing *EWS-FLI1* or eSZ expressing *EWS-CHOP* or *SYT-SSX1*.  $P < 0.02$  in eSZ/*EWS-FLI1* vs. eGP, eSyR, or shaft;  $P < 0.04$  in eSZ/*EWS-FLI1* vs. trunk and head, log-rank test. (C) Tumors were observed as subcutaneous masses in recipient nude mice. (D) Histology of murine Ewing's sarcoma. H&E staining, with low (left) and high (center) magnification. Pulmonary metastasis of murine Ewing's sarcoma developed by tail vein injection of tumor cells (right). Scale bar: 100  $\mu$ m. (E) Cre/*loxP*-mediated knockout of the *EWS-FLI1* transgene. Ewing's sarcoma developed by transplantation of eSZ cells transduced with the floxed *EWS-FLI1* retrovirus (left). Sarcoma cells were then maintained in vitro and transduced with the pMSCV-Cre retrovirus. Cre expression suppressed colony formation (right). The experiment was repeated 3 times and the representative results, are shown (graph inset). Scale bar: 100  $\mu$ m. \* $P < 0.01$ . The mean  $\pm$  SEM of 3 independent experiments is shown.

gene transfer of *EWS-FLI1* to all cell types by spin infection. The transduction efficiency was examined by flow cytometric analyses (Supplemental Figure 1A; supplemental material available online with this article; doi:10.1172/JCI72399DS1), and the expression of *EWS-FLI1* was confirmed by FACS and immunofluorescent staining using anti-FLAG (Supplemental Figure 1, B-D). One million transduced cells of each fraction were injected subcutaneously into nude mice. Recipients transplanted with eSZ cells transduced

with *EWS-FLI1* or *EWS-ERG* developed a subcutaneous mass at 100% penetrance, with a mean latency of 8 weeks (Figure 1, B-D).

As few as  $1 \times 10^4$  injected transduced eSZ cells could develop Ewing's sarcomas. In contrast,  $1 \times 10^6$  cells from *EWS-FLI1*-transduced eGP, embryonic shaft, or eSyR fractions were required for tumor development, clearly indicating that Ewing's sarcoma precursors were highly enriched in the eSZ fraction (Table 1). When embryonic mesenchymal cells purified from the mouse



**Table 1**  
Summary of the incidences of tumors in limiting dilution experiments using eSyR, eSZ, eGP, shaft, trunk, or head cells

Cells	Numbers of transplanted cells		
	1 × 10 <sup>6</sup>	1 × 10 <sup>5</sup>	1 × 10 <sup>4</sup>
eSZ	25/25 (100%)	12/13 (92%)	4/5 (80%)
eGP	3/9 (33%)	0/7 (0%)	ND
eSyR	2/12 (17%)	0/10 (0%)	ND
Shaft	1/9 (11%)	0/6 (0%)	ND
Trunk	3/9 (33%)	1/10 (10%)	0/5 (0%)
Head	2/9 (22%)	1/7 (14%)	0/5 (0%)

ND, not done.

head or trunk were transduced with *EWS-FLI1*, the incidence of small round cell sarcomas was again lower, and fibrosarcoma-like tumors were also obtained (Figure 1B and Supplemental Figure 2A). In addition, no tumor was induced when *EWS-CHOP* or *SYT-SSX1*, which are found in myxoid liposarcoma or synovial sarcoma, respectively, were introduced into eSZ cells (Figure 1B). Development of nonneoplastic bone and cartilage was observed when we transplanted eSZ cells treated with an empty vector (Supplemental Figure 2B).

Histological analysis showed that tumors expressing *EWS-FLI1* or *EWS-ERG* were composed of aggressively growing, small round cells, a feature typical of Ewing's sarcoma (Figure 1D). All the tumors examined (10 of 10) were capable of secondary transplantation (Supplemental Table 1 and Supplemental Figure 2C), and 3 of 9 tumors had metastatic potential by tail vein injection (Figure 1D, Supplemental Table 1, and Supplemental Figure 2D). *EWS-ETS* expression was confirmed by immunoblotting and immunostaining of FLAG-tagged proteins (Supplemental Figure 2E). MIC2 (also known as CD99), a surface marker for human Ewing's sarcoma (15), was focally detected (Supplemental Figure 2F). *Cd99* gene sequences are only partially conserved between human and mouse (16), and therefore, CD99 was not useful as a specific marker for murine Ewing's sarcoma.

*Cre/loxP*-mediated genetic recombination and knockout of the *EWS-FLI1* transgene induced complete growth arrest of the tumor (Figure 1E), and senescence-like cellular phenotypes were observed in 91.4% of surviving cells (1.4% in non-*Cre*-treated cells) (Supplemental Figure 3). Thus, murine Ewing's sarcoma is dependent on *EWS-FLI1* activity. These results indicate that cellular targeting of eSZ cells by *EWS-ETS* fusion genes efficiently and specifically induced human Ewing's-like sarcoma in mice.

In addition, the monoclonal or oligoclonal nature of murine Ewing's sarcoma was indicated by cloning of retroviral integration sites (Supplemental Excel File 1). The tumors ( $n = 21$ ) contained an average of 2.5 integration sites, and no common integration site has been identified, although there are interesting genes involved in neoplastic processes, such as *Ccnd3*, *Junb*, *Bach2*, and *Fyn*.

eSZ cells were characterized as osteochondrogenic progenitors. After condensation of mesenchymal stem/progenitor cells, the primitive structure of joint surfaces develops, and a chondrogenic progenitor lineage-rich eSZ emerges on the joint surface to develop the long bone from dpc 15.5 to P7 (Figure 2A and refs. 13, 17). eSZ cells purified by microdissection were positive for CD29 but lacked surface markers for MSC, such as SCA1, CD34, CD44, and

CD105, in contrast to embryonic trunk cells (Supplemental Figure 4A). eSZ cells were also negative for Gr-1, FLK1, and CD45 (Supplemental Figure 4A and data not shown). These data indicated that eSZ cells constituted a different cohort from those making up the previously defined MPC fraction that is positive for CD44, Thy1 (CD90), and SCA1 (9).

We compared gene expression profiles of purified eSZ and eGP cells obtained by microdissection. The results suggested that eSZ cells were an immature chondrogenic precursor (Supplemental Table 2 and Supplemental Excel File 2). Furthermore, laser microdissection, followed by expression analyses of a series of differentiation-related genes, was carried out to assess the gene expression profile of the eSZ fraction (Figure 2, B–D). As expected, *Erg* and growth/differentiation factor 5 (*Gdf5*) expression was prominent in eSZ cells. Moreover, eSZ cells showed gene expression profiles characteristic of immature chondrogenic precursors, including parathyroid hormone-like hormone (*Pthlh*), *Prg4*, and *Col2a1*, consistent with previous studies (Figure 2C and refs. 12, 18, 19). On the other hand, eGP cells showed a more differentiated chondrocytic gene expression profile, as represented by *Col10a1* (Figure 2C). Also, *Nanog*, *Oct4*, and *Sox2* (together denoted as NOS), which are expressed in most immature lineages, were enriched in eSyR, whereas little or no expression was observed in eSZ or eGP fractions. The results are summarized in Table 2, and they indicate that enrichment of an ERG<sup>hi</sup>/GDF5<sup>hi</sup>/PTHLH<sup>hi</sup>/PRG4<sup>hi</sup>/NOS<sup>lo</sup> fraction was achieved by fine selection of eSZ cells. *Gdf5* was transiently expressed in eSZ cells and is a master regulator of joint formation (20). *Gdf5* promoter activity was also exhibited exclusively in eSZ cells (Supplemental Figure 4B).

In an in vitro differentiation assay, eSZ cells exhibited remarkable osteogenic and chondrogenic differentiation potencies but lacked the ability to differentiate into the adipogenic lineage. In contrast, embryonic mesenchymal progenitor cells showed their typical multilineage differentiation pattern (Figure 2D). Adipogenesis-related genes, such as *Pparg* and *Fabp4*, were not expressed in eSZ cells, but they were observed in eSyR cells (Supplemental Figure 4C). Also, eSZ cells were unable to differentiate into myogenic or neuronal lineages (Supplemental Figure 4D).

The tumor induction efficiency was further enhanced by immune selection of the eSZ cells using PTHLH (Supplemental Figure 1D), a marker that is expressed by periarticular cells and articular chondrocytes (17, 21, 22). All the recipients transplanted with 1 × 10<sup>4</sup> PTHLH<sup>+</sup> eSZ cells developed Ewing's sarcoma with a significantly shorter latency than that of those receiving unselected eSZ cells ( $P < 0.01$ ). In contrast, no tumors were developed by recipients of the PTHLH<sup>-</sup> fraction of eSZ cells (Figure 2E; see complete unedited blots in the supplemental material). In addition, PTHLH<sup>+</sup> eSZ cells showed higher expression of *Erg* and *Gdf5* than the PTHLH<sup>-</sup> fraction (Figure 2F). These findings indicated that bipotential progenitors were present in the eSZ fraction and that successful enrichment of *Erg*<sup>+</sup> and *Pthlh*<sup>+</sup> progenitor cells was achieved in the eSZ cell fraction. eSZ cells were therefore used for the *EWS-ETS* gene transfer and subsequent transplantation experiments.

*Early neoplastic lesions of murine Ewing's sarcoma.* Our new animal model enabled us to examine how malignant cells progressed from preneoplastic and/or early neoplastic stages of cancer, stages that are difficult to observe in human Ewing's sarcoma (23). Early lesions of murine Ewing's sarcoma were therefore analyzed microscopically (Figure 3). Small foci of EWS-FLI1-positive (FLAG-positive) cells were observed adjacent to nonneoplastic cartilage (Figure 3A). Rapid cell cycle progression was confirmed in assess-

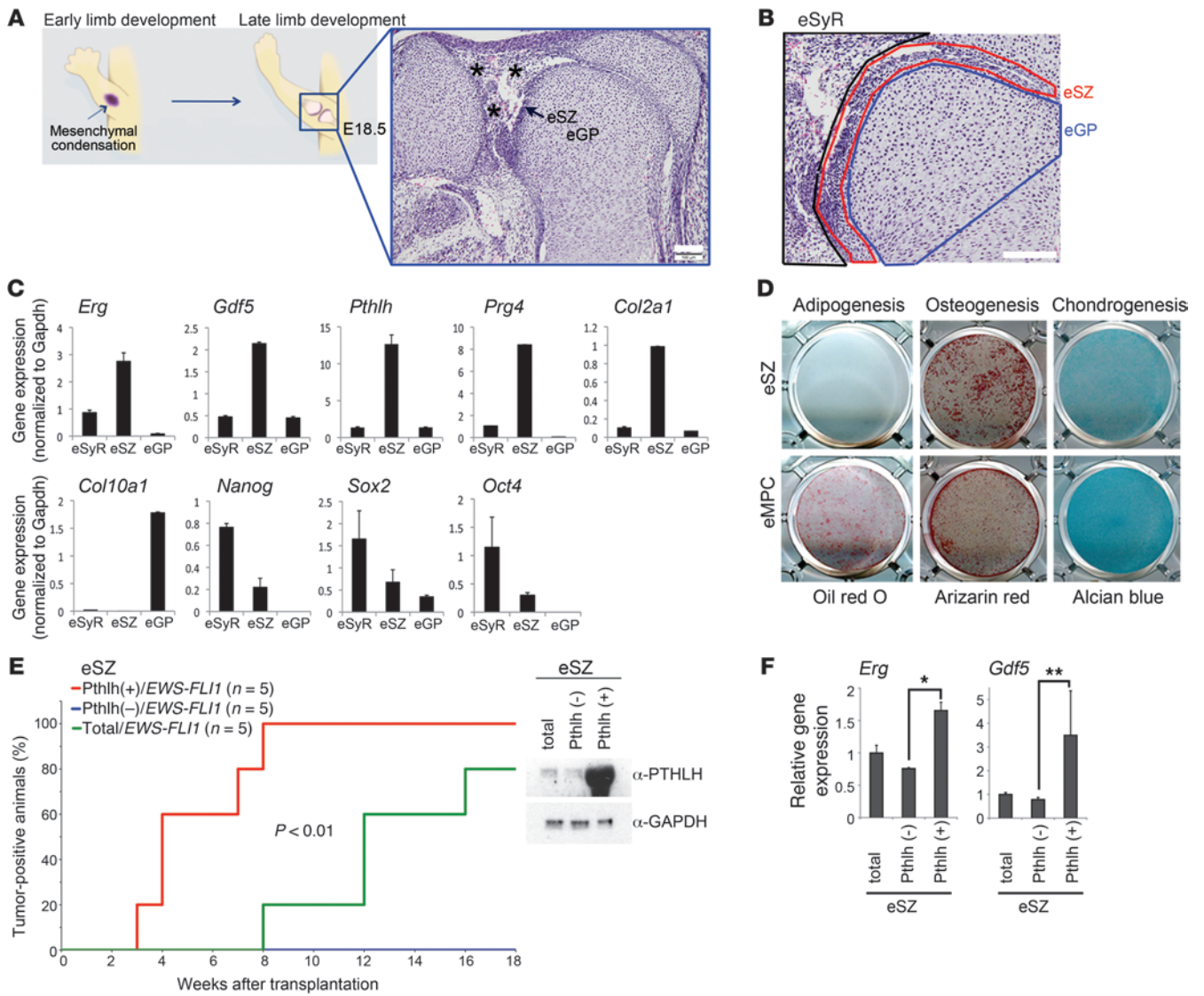


**Figure 2**

Characterization of eSZ cells. **(A)** Schematic illustration and histology of the developing knee joint in dpc 18.5 embryo. eSZ and eGP are indicated. Asterisks denote eSyR. Scale bar: 100  $\mu$ m. **(B)** eSZ, eGP, and eSyR components were fractionated by laser microdissection and subjected to gene expression analysis. Scale bar: 100  $\mu$ m. **(C)** Differentially expressed genes among eSyR, eSZ, and eGP cells. Quantitative RT-PCR analysis for *Erg*, *Gdf5*, *Pthlh*, *Prg4*, *Col2a1*, *Col10a1*, *Nanog*, *Sox2*, and *Oct4* expression in eSyR, eSZ, and eGP cells. The mean  $\pm$  SEM of 3 independent experiments are shown. **(D)** In vitro differentiation assays of eSZ cells and trunk mesenchymal progenitor cells (eMPC). Adipogenic, osteogenic, and chondrogenic differentiation was induced in embryonic mesenchymal progenitor cells, whereas eSZ cells showed no adipogenic differentiation. The experiment was repeated 3 times, and representative results are shown. **(E)** PTHLH<sup>+</sup> and PTHLH<sup>-</sup> fractions were separated using biotinylated anti-PTHLH and avidin-conjugated magnetic beads. Tumor induction was examined by transplantation of each fraction ( $1 \times 10^4$  cells).  $P < 0.01$  in PTHLH<sup>+</sup> eSZ/EWS-FLI1 vs. total eSZ, log-rank test. Condensation of the PTHLH<sup>+</sup> fraction was confirmed by immunoblotting. **(F)** Expression of *Erg* and *Gdf5* in PTHLH<sup>+</sup> and PTHLH<sup>-</sup> eSZ cells. The mean  $\pm$  SEM of 3 independent experiments are shown. \* $P < 0.01$ ; \*\* $P < 0.05$ .

ments of BrdU incorporation (Figure 3B). The early neoplastic lesions did not express neural, myogenic, epithelial, vascular, or hematopoietic markers, including CD57, NGFR, S-100, myosin, desmin, von Willebrand factor, cytokeratin, or CD45 (data not shown). A few FLAG-positive cells expressed collagen type 2, a marker of immature chondrocytes (18, 24), and were observed in the peripheral areas around the early neoplastic foci (Figure 3C). Interestingly, these differentiating cells exhibited cytoplasmic staining for EWS-FLI1. Staining was essentially localized to the

nucleus in the central part of the early neoplastic lesion (Figure 3B). Whereas nuclear localization of EWS-FLI1 fusion protein has been confirmed in most cell types (25), its cytoplasmic localization in differentiating cells suggests that cytoplasmic exclusion of EWS-FLI1 might represent an inhibitory mechanism in tumorigenesis of Ewing's sarcoma. The existence of cytoplasmic exclusion suggests that EWS-FLI1 expression alone is insufficient to induce complete tumorigenesis. In addition, more differentiated chondrocytes, positive for S100 or collagen type 10, were observed



**Table 2**  
Summary of eSZ cell profiles

Gene	Expression properties	
	Levels in eSZ	Other mesenchymes
<i>Erg</i>	High	SZ (E)
<i>Gdf5</i>	High	SZ (E)
<i>Pthlh</i>	High	SZ (E, A)
<i>Prg4</i>	High	SZ (E, A)
<i>Col2a1</i>	Moderate	Proliferating chondrocytes (E, A)
<i>Col10a1</i>	None	Hypertrophic chondrocytes (E, A)
<i>Nanog</i>	Low	ES, EMPC
<i>Sox2</i>	low	ES, EMPC
<i>Oct4</i>	low	ES, EMPC

SZ, superficial zone or articular cartilage; ES, embryonic stem cell; EMPC, embryonic mesenchymal progenitor cell. Parenthetical E or A indicate embryo or adult, respectively.

in the surrounding area (Figure 3D and Supplemental Figure 5). EWS-FLI1 expression was hardly detected in S100-positive cells (Figure 3D). Microdissection and gene expression analyses of early neoplastic lesions revealed continued expression of *Erg*, *Gdf5*, *Pthlh*, and *Prg4*, whereas, in differentiated areas, downregulation of those genes was accompanied by increased *Col10a1* expression (Figure 3E). Those results indicated that the nature of the eSZ is preserved in the early neoplastic lesion, at least in part.

*Murine Ewing's sarcoma shared common gene expression profiles with human small round cell tumor, including Ewing's sarcoma and neuroblastoma.* Expression profiles of murine Ewing's sarcomas were compared with those of a series of human sarcomas, including Ewing's sarcoma, malignant fibrous histiocytoma, myxoid liposarcoma, synovial sarcoma, osteosarcoma, neuroblastoma, and chondrosarcoma. Hierarchical clustering using common gene sets between mice and humans (1,819 probes selected from 23,860 probe sets) showed that the murine Ewing's sarcoma was quite similar to the human Ewing's sarcoma and neuroblastoma (Figure 4A). The results suggested a relationship between the present model and human Ewing's sarcoma. Moreover, the neuroblastoma-like small round cell morphology could be induced from osteochondrogenic precursor cells by *EWS-FLI1* expression.

To better understand the nature of the small round tumor cells, the expression profile of mouse Ewing's sarcoma was again compared with that of human Ewing's sarcoma, poorly differentiated synovial sarcoma, neuroblastoma, and malignant lymphoma, and the profile of human Ewing's sarcoma was compared with that of mouse tumors (Figure 4B). Two thousands probe sets "specific" for each tumor that showed larger differences of expression relative to the rest of the tumor types were selected in both human and mouse tumor groups. Then, lists of the 2,000 probes were compared between mouse Ewing's sarcoma and each human tumor and between human Ewing's sarcoma and each mouse tumor, resulting in the selection of human and mouse Ewing's sarcoma as the closest counterparts to each another (Figure 4B), though the data were not statistically significant except for malignant lymphoma. Collectively, these data indicate that the expression profiles depend in part on the cell morphology of the small round cell tumor. It is notable that EWS-FLI1 expression in murine eSZ cells could induce human Ewing's sarcoma-like gene expression profiles.

Common upregulated genes in murine and human Ewing's sarcoma are presented in Supplemental Excel File 3 and Supplemental Figure 6A. The analysis revealed that 336 genes were upregulated in both murine and human Ewing's sarcomas, including known EWS-FLI1 targets such as *Dkk2*, *Prkcb1*, enhancer of zeste homolog 2 (*Ezh2*), *Id2*, *Nkx2.2*, *Nr0b1*, and *Ptpn13* (26–32). Furthermore, 6,014 genes, including EWS-FLI1 targets such as *Aurka*, *Gstm4*, *Tert*, *Tnc*, and *Upp1*, were upregulated in murine Ewing's sarcoma (Figure 4C, Supplemental Excel File 3, and refs. 33–37). These 5 genes were identified by EWS-FLI1 overexpression or silencing studies or by an immunohistochemical analysis that might cause exclusion of them as upregulated genes in human Ewing's sarcoma. Twenty-two out of thirty upregulated targets proposed by Ordonez et al. (8) were indeed upregulated in our model. In addition, 360 genes (including *Tgfb2*) (38) were downregulated in both murine and human Ewing's sarcoma (Supplemental Figure 6A and Supplemental Excel File 4). These genes were potentially EWS-FLI1-responsive genes and might be important in the early oncogenic process as well as in the progression toward more malignant phenotypes. These gene expression results support the authenticity of our murine model for human Ewing's sarcoma.

The same analysis showed that 129 genes were upregulated in both murine and human Ewing's sarcoma as well as human neuroblastoma. Upregulation of a series of neuronal differentiation-related genes (*Gfra2*, *Ncan*, *Nrxn1*, and *Ntrk1*) and synapse-related genes (Supplemental Figure 6B) in murine Ewing's sarcoma was also observed in human neuroblastoma, indicating that the neuronal phenotype could be induced from osteochondrogenic progenitors, probably through transdifferentiation processes. The neuroectodermal-related signaling pathway, including NTRK1/NTRK3 and N-MYC, might play some role in neuronal phenotypes of Ewing's sarcoma. Although the number of commonly upregulated genes in murine Ewing's sarcoma and neuroblastoma was larger than that in murine and human Ewing's sarcoma, most of the known target genes described above were included in the latter category, suggesting that the core mechanisms of EWS-FLI1 transcriptional regulation might be preserved in our model.

*EWS-FLI1-responsive genes and chromatin modification in eSZ cells.* The relationship between the cell of origin of Ewing's sarcoma and *EWS-ETS* fusions is important, given the strict limitations on the origin of murine Ewing's sarcoma. Gene expression profiles were therefore compared between eSZ and eGP cells in the presence or absence of *EWS-FLI1* (Figure 5A and Supplemental Excel File 5) (data are available at NCBI Gene Expression Omnibus [GEO] with accession number GSE32618). Most of the known EWS-FLI1 target genes (8) were upregulated in eSZ cells following *EWS-FLI1* introduction (Supplemental Excel File 5). *EWS-FLI1* encodes an aberrant transcription factor (8, 30), and the response to it differed between eSZ and eGP cells (Figure 5B, Supplemental Figure 7, and Supplemental Excel File 6). The different gene responses in eSZ and eGP cell fractions were probably caused by differences in chromatin conditions at target loci. Histone modifications were therefore examined on representative genes, such as *Dkk2*, *Prkcb1*, and *Ezh2*. Histones H3K9/K14ac and H3K4me, which are activation marks for gene expression, were observed predominantly in eSZ cells as well as mouse Ewing's sarcoma cells, whereas histone H3K9me3 and H3K27me3, which are repressive marks, were observed predominantly in eGP cells (Figure 5C). These results strongly suggest that transcriptional activation of EWS-ETS target genes occurred in eSZ cells at maximum efficiency and that

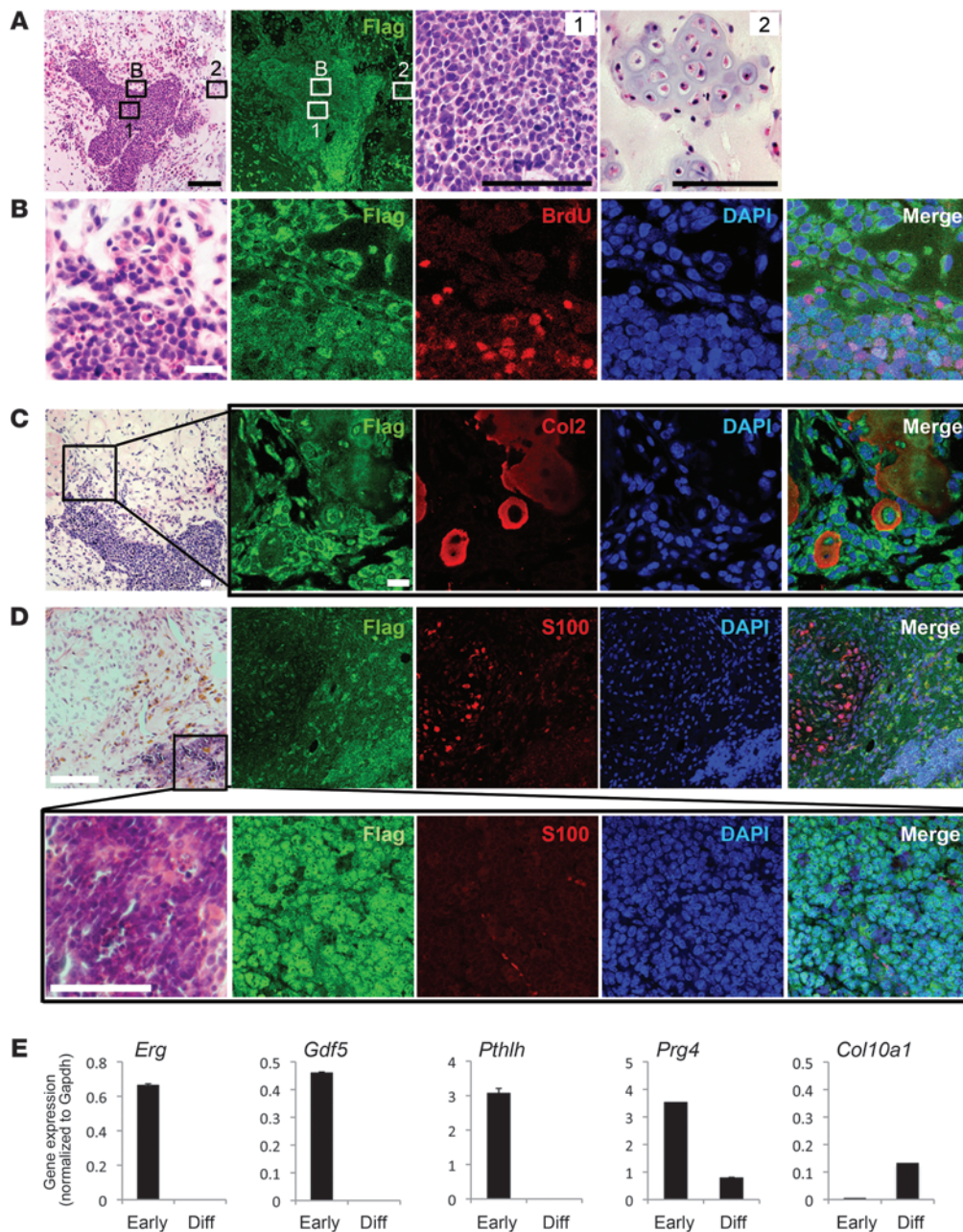


**Figure 3**

An early neoplastic lesion of murine Ewing’s sarcoma 3 weeks after transplantation. **(A and B)** Immunofluorescent assessment of FLAG. **(A)** High-power images of early neoplastic cells (see boxed region 1 shown at higher magnification) and nonneoplastic cartilage (see boxed region 2 shown at higher magnification) are shown. Scale bar: 100  $\mu$ m. **(B)** The boxed region in **A** shown at higher magnification. Accumulation of BrdU-positive nuclei in the central early neoplastic lesions. Nuclear localization of EWS-FLI1 (FLAG) was observed in the central region, whereas cytoplasmic translocation of EWS-FLI1 is remarkable in the differentiating zone. Scale bar: 20  $\mu$ m. **(C)** The differentiating zone with cytoplasmic EWS-FLI1 staining is characterized by collagen 2 expression. Scale bar: 20  $\mu$ m. **(D)** Further differentiation toward the chondrogenic lineage in a more peripheral area is indicated by expression of S100 (top row), which is negative in the central early neoplastic lesion (bottom row). Scale bar: 100  $\mu$ m. **(E)** Quantitative real-time PCR analysis for *Erg*, *Gdf5*, *Pthlh*, *Prg4*, and *Col10a1* expression in early neoplastic cells and the differentiating zone. The mean  $\pm$  SEM of 3 independent experiments are shown.

the histone status in eSZ cells was preserved after transformation, thereby providing the aggressive oncogenic function of EWS-ETS.

*Upregulation of the WNT/ $\beta$ -catenin pathway in eSZ cells and in Ewing’s sarcoma cells.* Gene set enrichment analyses (GSEA) using

gene sets of *EWS-FLI1*-expressing eSZ and eGP cells 48 hours after gene introduction exhibited enrichment of genes within the WNT/ $\beta$ -catenin pathway as well as the EGF and RTK signaling pathways (Figure 6A and Supplemental Figure 7). In the



WNT/ $\beta$ -catenin pathway, the expression of *Dkk2* and *Wif1* was observed in eSZ cells expressing *EWS-FLI1* (Figure 5B and Figure 6B). *Dkk2* expression was comparable between parental eSZ and eGP cells, and *EWS-FLI1* introduction induced upregulation of *Dkk2* only in eSZ cells (Figure 5B and Figure 6B). In contrast, expression of *Dkk1*, which is antagonistic to DKK2, remained unaltered by *EWS-FLI1* introduction in eSZ cells. Higher *Wif1* expression was observed in eSZ cells but not in eGP cells, and the difference in expression between eSZ and eGP cells was preserved after *EWS-FLI1* introduction. The WNT/ $\beta$ -catenin pathway was not enriched when gene sets of nontransduced eSZ and eGP cells were tested (data not shown). In addition, gene sets for the EGF pathway and receptor protein kinase activity were enriched (Figure 6B and Supplemental Figure 8). *Prkcb1* is a gene downstream from *EWS-FLI1* (39) and is inherently expressed at higher levels in eSZ cells than in eGP cells. Notably, its expression was increased to higher levels by introducing *EWS-FLI1* into eSZ cells. *Flt4* (also known as *VEGFR3*) and *Musk*, which are important in signaling of vascular and neuromuscular systems, were also identified as *EWS-FLI1*-responsive genes (Figure 6B and Supplemental Figure 8). Furthermore, IGF1R and IGF2R, which are involved in IGF1 signaling and are attractive targets in Ewing's sarcoma therapy (40, 41), were also identified by GSEA (Supplemental Figure 8).

*Dkk2* is a member of the dickkopf family of proteins. As modulators of the WNT/ $\beta$ -catenin pathway, this family plays important roles in the development and homeostasis of bone and cartilage (42). A previous study showed that *DKK2* was downregulated upon *EWS-FLI1* knockdown in Ewing's sarcoma cells, while the opposite response was observed in *DKK1* (26). Although previous studies suggested that *DKK1* and *DKK2* might have functions independent of the canonical WNT/ $\beta$ -catenin pathway (43), possible roles of WNT activation in human Ewing's sarcoma were reported (44).

To confirm the involvement of the WNT/ $\beta$ -catenin pathway in tumorigenesis of Ewing's sarcoma, expression of  $\beta$ -catenin protein was evaluated.  $\beta$ -Catenin expression was increased by transient introduction of *EWS-FLI1* into eSZ cells (Supplemental Figure 9A). As described above, murine Ewing's sarcoma was serially transplantable into syngeneic mice and showed high potency of proliferation (Supplemental Figure 2C). In the invasive area of the secondary tumor, increased expression of  $\beta$ -catenin was frequently observed (Supplemental Figure 9B). RNA interference-mediated *EWS-FLI1* knockdown resulted in decreased transcriptional activities of  $\beta$ -catenin (Supplemental Figure 9C). Collectively, these data indicate strong association between the upregulation of WNT/ $\beta$ -catenin signaling and cell growth of Ewing's sarcoma.

*Inhibition of tumor growth by suppression of critical signals.* The result indicates that *EWS-FLI1* and its downstream signals are effective targets for therapy. Indeed, gene knockdown experiments showed that tumor cell proliferation was significantly inhibited by siRNA treatments specific for *Fli1*, *Dkk2*, *Catnb*, *Prkcb1*, *Ezh2*, or *Igf1* (Figure 6C). Knockdown of the same genes in the human Ewing's sarcoma cells showed similar suppression of cell proliferation (Supplemental Figure 10). Moreover, suppression of the EGF/RAS/MAPK pathway by a MEK1 inhibitor (U0126) showed inhibition of tumor growth in vitro in a dose-responsive manner (Figure 6D). These results demonstrated the importance of the signaling pathways activated by *EWS-FLI1* in the progression of Ewing's sarcoma and its potential as a novel target for clinical treatment.

*Use of the mouse model to test therapy targeted against Ewing's sarcoma.* Animal models of human cancer provide platforms for evaluation of novel therapies. Ideally, the phenotypes and developmental mechanisms of the human and model systems should be similar. In this context, specific inhibitors of the WNT/ $\beta$ -catenin pathway, EZH2 and poly (ADP-ribose) polymerase 1 (PARP1), were tested using the current model both in vitro and in vivo. The  $\beta$ -catenin inhibitors, iCRT14 and PNU74654, showed marked growth suppression of both mouse and human Ewing's sarcoma, and an EZH2 inhibitor DZNeP showed modest but substantial growth suppression (Figure 7A and Table 3). Moreover, olaparib, a PARP1 inhibitor reported to exhibit Ewing's sarcoma-specific growth inhibition (45), also inhibited both mouse and human Ewing's sarcomas (Figure 7A and Table 3). Cell cycle analyses showed that iCRT14 and DZNeP induced cell cycle arrest, as indicated by increased  $G_1$  populations and decreased  $G_2/M$  populations (Figure 7B). PNU74654 and olaparib also increased a sub- $G_1$  population, indicating apoptosis induction (Figure 7B). These reagents also suppressed in vivo growth of Ewing's sarcoma, with the greatest effect observed with iCRT14, followed by olaparib, DZNeP, and PNU74654 (Figure 7C). Thus, the current model provides an effective tool to explore and evaluate novel therapeutic drugs both in vitro and in vivo.

## Discussion

Here, we demonstrate efficient and specific induction of a mouse equivalent of human Ewing's sarcoma. We showed that the origin of the tumor is closely related to embryonic osteochondrogenic progenitor cells. Selection of a PTHLH-expressing cellular fraction in eSZ enabled us to obtain substantially higher efficiency and greater specificity and consistency of tumor formation than previously reported investigations using bone marrow-derived mesenchymal stem/progenitor cells (9, 10). In addition, *EWS-FLI1* expression induced apoptosis and growth arrest in several cell types, including embryonic fibroblasts (46, 47). These data indicate that induction of Ewing's sarcoma by *EWS-ETS* fusion genes is much more effective for progenitor cells of a certain cell lineage, including the osteochondrogenic axis, especially in developing bone. A previous study indicated that *EWS-FLI1* induces cancer stem cell properties in pediatric MSCs but not in adult MSCs (48). The plasticity for cellular differentiation in embryonic and pediatric precursor cells might be important for Ewing's sarcoma development in younger patients. Moreover, *EWS-ETS* might induce the development of small round cells and neuroectoderm-like phenotypes.

Ewing's sarcoma is a rather rare neoplasm that affects children and adolescents with an incidence of 2.1 cases per million children (49). The low incidence of disease is also observed in other translocation-related sarcomas affecting young people, such as alveolar rhabdomyosarcoma, clear cell sarcoma, synovial sarcoma, or myxoid liposarcoma (50). This is in contrast to acute myeloid leukemia (AML), which is also characterized by gene fusion. It is likely that the difference in frequencies between sarcomas and AMLs is due to the rarity of progenitor cell populations in which chromatin conditions necessary for the oncogenic action of *EWS-ETS* are present. Such a narrow window of target cell emergence reflects the difficulty of inducing tumor in vivo models.

Once the *EWS-FLI1* fusion occurs in an eSZ cell during the perinatal period or even in utero, the cell survives with acquired growth advantages. After a decade of incubation that allows additional genetic/epigenetic events in the mutated eSZ cell, Ewing's sarcoma eventually emerges in the bone as a highly aggressive tumor in human child-

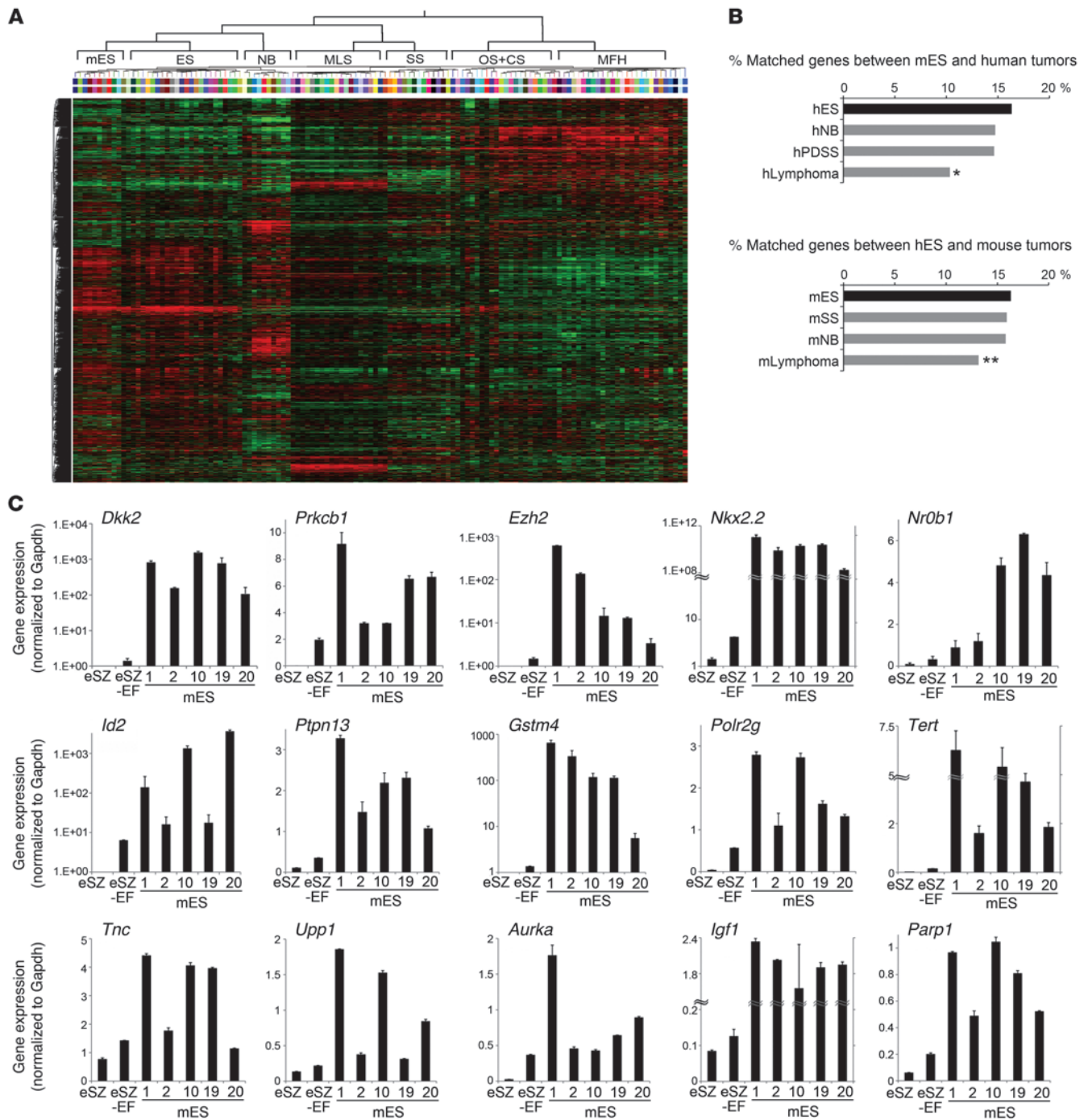


**Figure 4**

Clustering analysis of murine and human sarcomas. **(A)** Supervised clustering of gene expression profiles of 10 samples of murine Ewing’s sarcomas (mES), 32 cases of human Ewing’s sarcomas (ES), 21 malignant fibrous histiocytomas (MFH), 20 myxoid liposarcomas (MLS), 16 synovial sarcomas (SS), 11 osteosarcomas (OS), 10 neuroblastomas (NB) and 7 chondrosarcomas (CS). **(B)** Gene expression profiles of mouse and human Ewing’s sarcoma (hES) were compared with those of other small round cell tumors of the other species. The frequencies of matched genes in 2,000 gene sets are indicated. Expression profiles of 6 human poorly differentiated synovial sarcoma (hPDSS) cases, 14 cases of human malignant lymphoma, 5 samples of murine synovial sarcoma, 7 murine neuroblastomas, and 6 murine malignant lymphoma were examined. **(C)** Quantitative RT-PCR for upregulated genes common between eSZ cells with *EWS-FLI1* (EF) and murine Ewing’s sarcomas. The numbers listed above “mES” denote tumor IDs. The mean ± SEM of 3 independent experiments are shown. \**P* < 0.001 vs. hES; \*\**P* < 0.01 vs. mES.

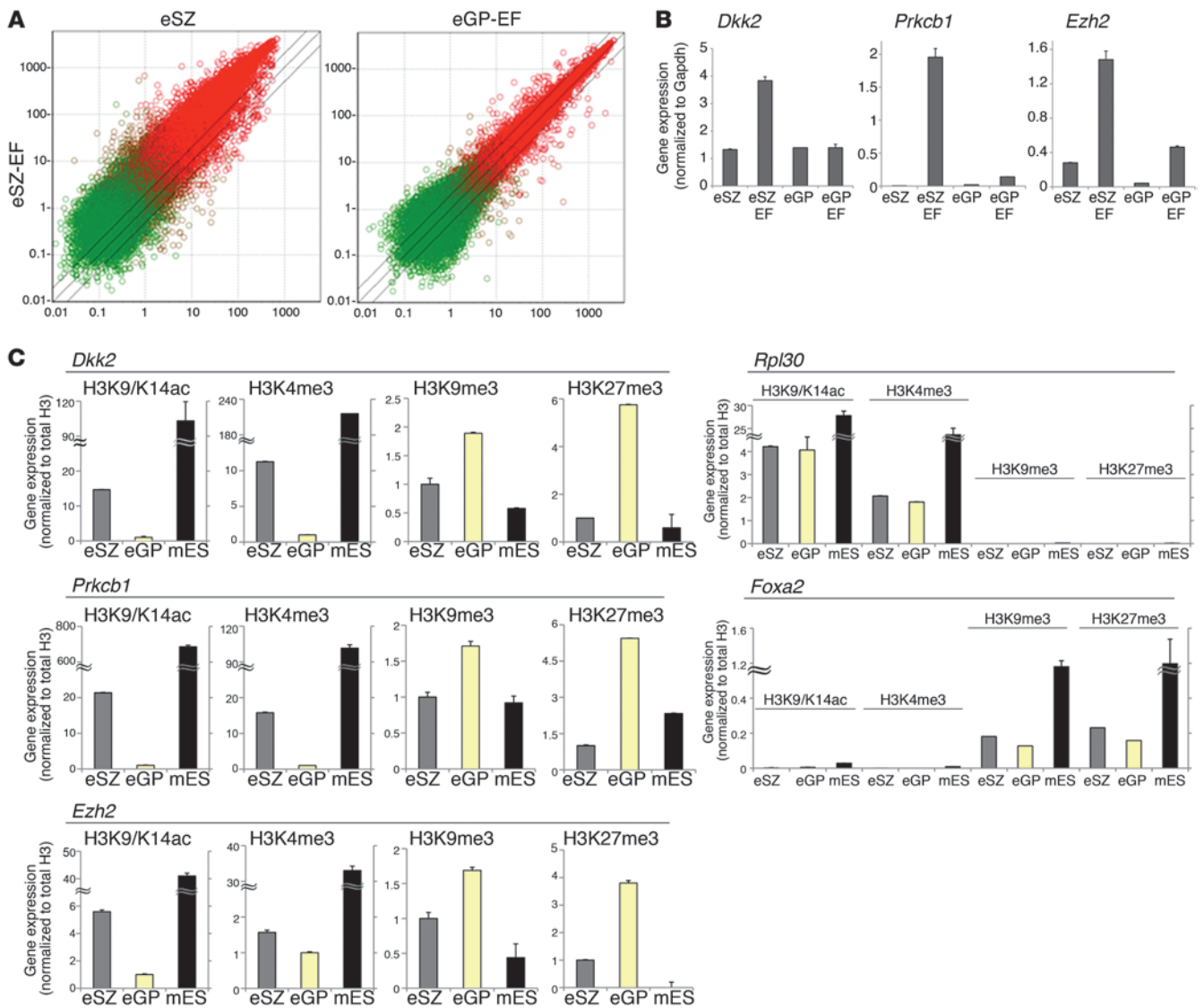


**Figure 5** Differences in gene expression between eSZ and eGP cells. **(A)** Comparison of gene expression profiles between eSZ/*EWS-FLI1* and eSZ and eSZ/*EWS-FLI1* and eGP/*EWS-FLI1* 48 hours after introduction. Scatter plots of eSZ with (vertical axis) or without *EWS-FLI1* (horizontal axis) and eSZ with *EWS-FLI1* (vertical axis) or eGP with *EWS-FLI1* (horizontal axis) are shown. Red dots indicate probes of present call, and green dots indicate those of absent call. The threshold lines above and below the diagonal indicate  $y = 2x$  (2-fold increase) and  $y = 0.5x$  (2-fold decrease), respectively. **(B)** Expression patterns of *Dkk2*, *Prkcb1*, and *Ezh2* were validated by quantitative RT-PCR. The mean  $\pm$  SEM of 3 independent experiments are shown. **(C)** ChIP-PCR for histone modification at *Dkk2*, *Prkcb1*, and *Ezh2* promoter regions in eSZ, eGP, and murine Ewing’s sarcomas. *Rpl30* and *Foxa2* were used as controls for active and repressive histone marks, respectively. The mean  $\pm$  SEM of 3 independent experiments are shown.

hood. This scenario explains why the location of Ewing’s sarcoma is different from that of osteosarcoma, which is frequently observed in the metaphysis of long bones. There is a variant of human Ewing’s sarcoma that develops in the soft tissue and is also characterized by the invariable *EWS-ETS* fusion. As the origin of Ewing’s sarcoma in the soft tissue remains to be clarified, the relatively late onset of the tumor suggests that dysregulation of the differentiation program in the mesenchymal system might play some role in its tumorigenesis.

Upregulation of the WNT/ $\beta$ -catenin pathway is a direct effect of *EWS-ETS* expression in preneoplastic and sarcoma cells, at least in part. However, rather mild  $\beta$ -catenin induction by

*EWS-FLI1* in the eSZ (Supplemental Figure 9A) suggests that additional genetic events might be required for constitutive activation of the pathway. Pathways involving receptor tyrosine kinases are also important in Ewing’s sarcoma (40, 51), as was indicated in our model. Indeed, potential clinical benefits from the use of pazopanib, a multikinase inhibitor, for the treatment of childhood sarcoma, including Ewing’s sarcoma, have been reported recently (52).

Tumor formation in our mouse model of Ewing’s sarcoma was *EWS-ETS* dependent, as was clearly exhibited by *Cre/loxP*-mediated knockout experiments. This finding suggests that therapeutic

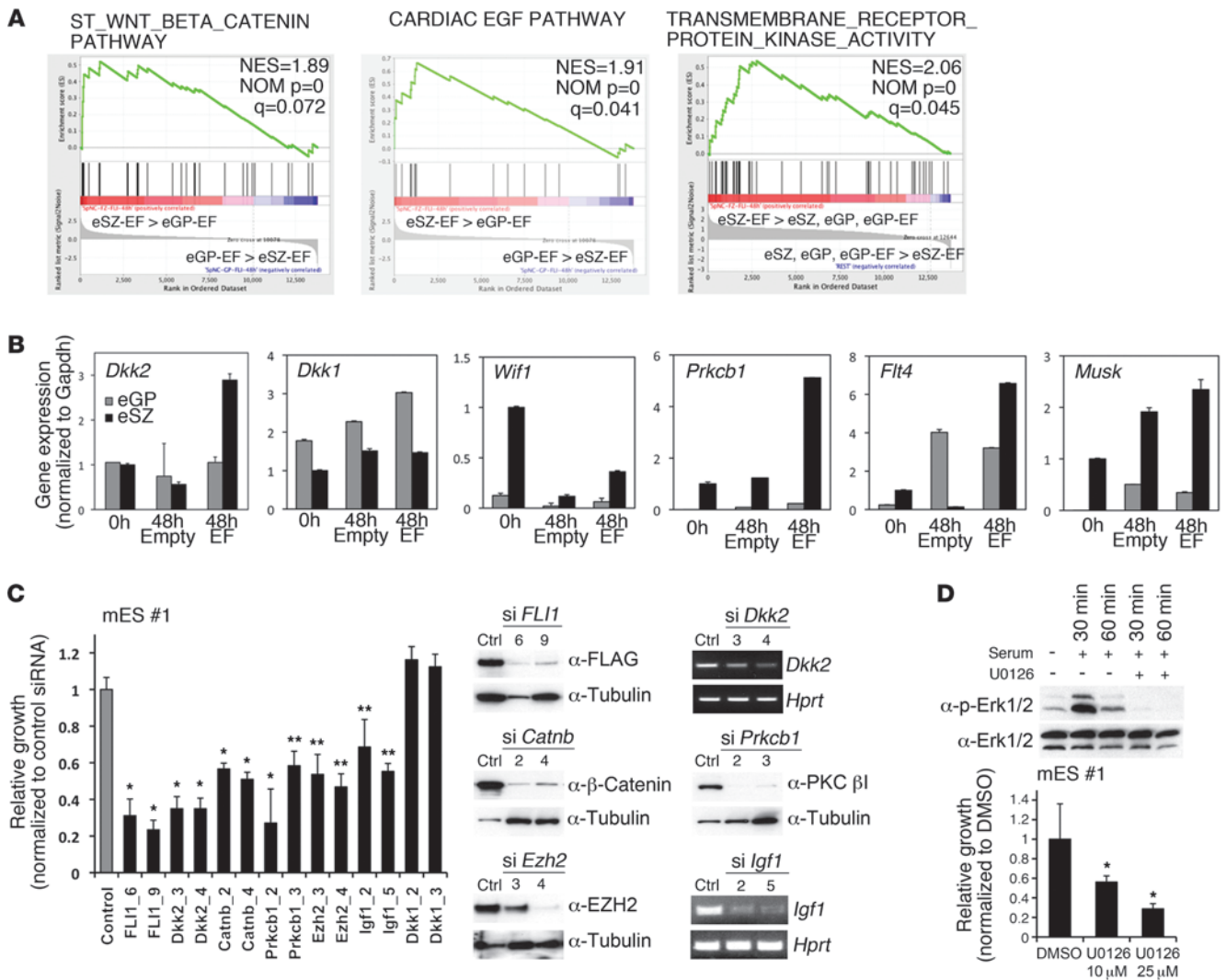


**Figure 6** Modulation of gene expression and growth suppression of tumor cells by gene silencing. (A) GSEA of eSZ and eGP cells with *EWS-FLI1* (left and central panels) and between eSZ/*EWS-FLI1* and eGP, eSZ, and eGP/*EWS-FLI1* (right) resulted in enrichment of the WNT/ $\beta$ -catenin pathway, the EGF pathway, and receptor tyrosine kinase activities. (B) Real-time quantitative RT-PCR for *Dkk2*, *Dkk1*, *Wif1*, *Prkcb1*, *Flt4*, and *Musk* in eSZ or eGP cells with/without *EWS-FLI1* at 0 or 48 hours after introduction. The mean  $\pm$  SEM of 3 independent experiments are shown. (C) Inhibition of cell proliferation by knockdown of *EWS-FLI1* and genes of the pathways specified in A. Relative growth of tumor cells 48 hours after siRNA treatment was calculated by comparing each cell number to cells treated with control siRNA. The symbols of siRNA used are indicated. *Dkk1* was tested as a negative control. Gene knockdown was confirmed by immunoblotting (*Flt1*, *Catnb*, *Ezh2*, and *Prkcb1*) or RT-PCR (*Dkk2* and *Igf1*). The experiment was repeated 3 times, and representative results are shown. (D) Effect of MAPK pathway inhibition on tumor growth. Erk phosphorylation was inhibited by a MEK1/2 inhibitor U0126 (10  $\mu$ M) (top), and tumor proliferation was inhibited in a dose-dependent manner 48 hours after treatment (bottom). The mean  $\pm$  SEM of 3 independent experiments are shown. \* $P < 0.01$ ; \*\* $P < 0.02$ .

approaches should pursue the direct targeting of EWS-ETS as well as related pathways. Gene knockdown experiments and screening of inhibitory drugs in our model should prove valuable. Unlike the xenograft model of human cancer cells, the present mouse model excludes the unexpected bias caused by rather low penetrance of transplantation, an altered relationship between tumor cells and the microenvironment, and defects in certain signaling pathways due to differences in species-dependent binding affinities between ligands and receptors. Thus, our platform will allow us to explore and evaluate novel targeted therapies in combination with tests using human Ewing's sarcoma cell lines.

In summary, purification of the targets of primary oncogenic stimuli permitted us to establish a mouse model that closely recapitulates important characteristics of human Ewing's sarcoma. Taken together, the efficiency of tumor induction and the gene expression analyses of both the very limited cell population obtained by laser microdissection and the early neoplastic lesion strongly suggest that the cell of origin of Ewing's sarcoma is enriched in the eSZ cells. The present ex vivo method could be useful for generating other important animal models for human cancers, particularly when conventional transgenic models are driven by a gene expression-based method that is not always successful at

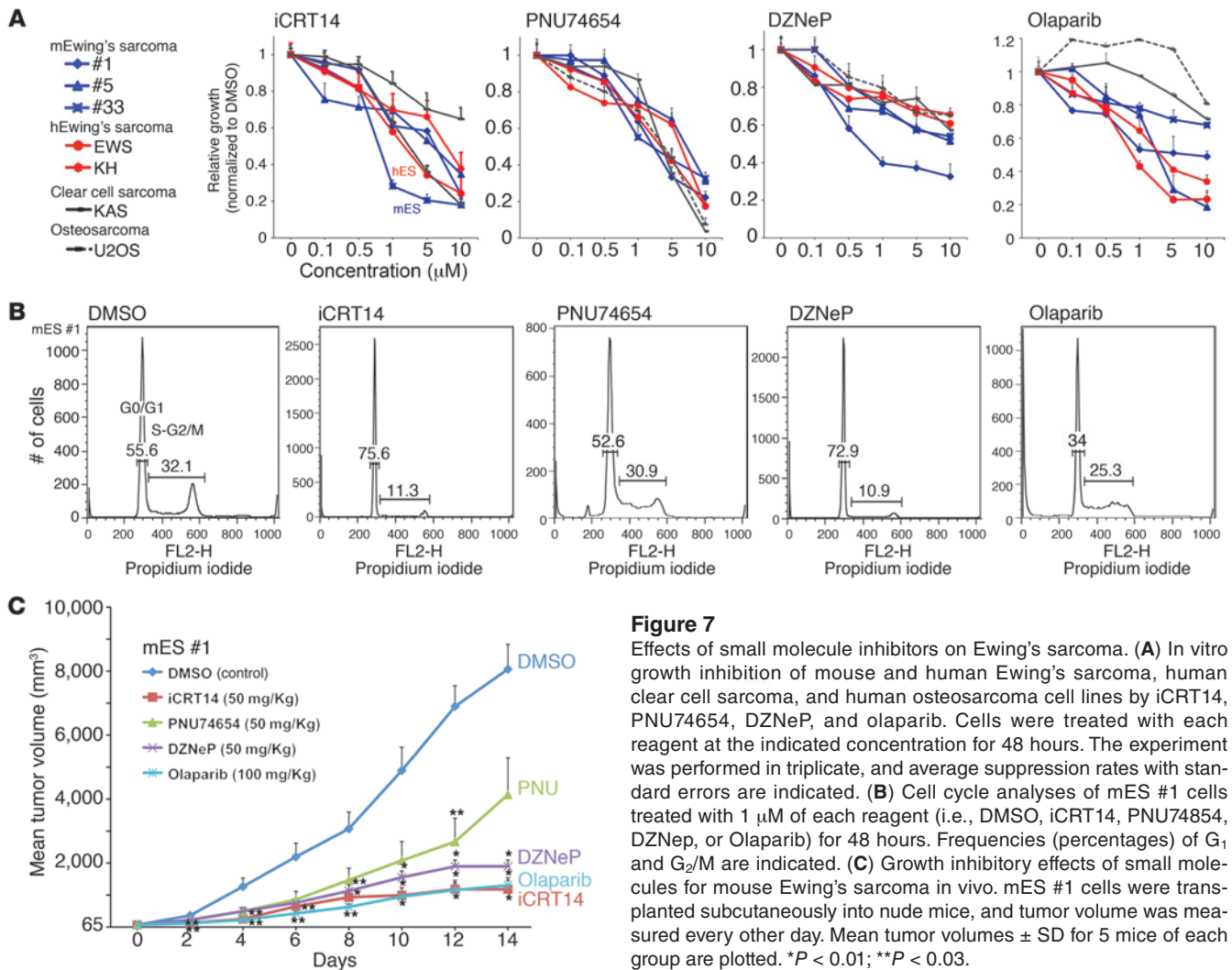


**Figure 7**

Effects of small molecule inhibitors on Ewing's sarcoma. **(A)** In vitro growth inhibition of mouse and human Ewing's sarcoma, human clear cell sarcoma, and human osteosarcoma cell lines by iCRT14, PNU74654, DZNeP, and olaparib. Cells were treated with each reagent at the indicated concentration for 48 hours. The experiment was performed in triplicate, and average suppression rates with standard errors are indicated. **(B)** Cell cycle analyses of mES #1 cells treated with 1  $\mu\text{M}$  of each reagent (i.e., DMSO, iCRT14, PNU74654, DZNeP, or Olaparib) for 48 hours. Frequencies (percentages) of G<sub>1</sub> and G<sub>2</sub>/M are indicated. **(C)** Growth inhibitory effects of small molecules for mouse Ewing's sarcoma in vivo. mES #1 cells were transplanted subcutaneously into nude mice, and tumor volume was measured every other day. Mean tumor volumes  $\pm$  SD for 5 mice of each group are plotted. \* $P < 0.01$ ; \*\* $P < 0.03$ .

targeting exact cell types. The plasticity of precursor cells as well as their oncogenic potency due to chimeric transcription factors can be evaluated by the present approach and constitutes a useful tool for clarifying oncogenic mechanisms of childhood cancer.

**Methods**

**Purification of eSZ cells.** Femoral and humeral bones of BALB/c mouse embryos were removed aseptically on 18.5 dpc, and they were microdissected into eSZ, eGP, and eSyR under a stereomicroscope (Zeiss Stemi 2000-C, Carl Zeiss MicroImaging). Embryonic mesenchymal cells of the head or trunk were also prepared from the same embryos during each experiment. Each region was minced and gently digested with 2 mg/ml collagenase (Wako Pure Chemical) at 37°C for 2 hours. They were cultured in growth medium composed of Iscove's Modified Dulbecco's Medium (Invitrogen) supplemented with 15% fetal bovine serum and subjected immediately to retroviral infection. Fractionation of PTHLH<sup>+</sup> and PTHLH<sup>-</sup> eSZ populations was achieved using a rabbit anti-PTHLH (Abcam) and a CELlection Biotin Binder Kit (Dyna) according to the manufacturer's protocol. The frequency of the PTHLH<sup>+</sup> cells reached 8.3% of total eSZ cells (12-fold enrichment).

**Retroviral infection and transplantation.** N-terminal FLAG-tagged *EWS-FLI1* and *EWS-ERG* were introduced into the pMYS-IRES-GFP or pMYS-IRES-Neo vectors. The full-length *EWS-FLI1* cDNA was a gift from Susanne

Baker (St. Jude Children's Research Hospital, Memphis, Tennessee, USA), and *EWS-ERG* was cloned from a human Ewing's sarcoma case. Retroviral infections of eSZ, eGP, or shaft cells were performed as described previously (53). Infection efficiency was examined using a FACSCalibur flow cytometer (Becton Dickinson). After 48 hours of spin infection, the cells were mixed with growth factor-reduced Matrigel (Becton Dickinson) and were transplanted subcutaneously to BALB/c nude mice. The mice were observed daily to check for tumor formation and general condition. Tumors were resected and subjected to further examination when subcutaneous masses reached 15 mm in diameter. Some tumors ( $1 \times 10^6$  cells) were serially transplanted subcutaneously or injected into the tail veins ( $1 \times 10^6$  cells) of nude mice to confirm tumorigenicity and metastatic activities.

**Histopathology and immunohistochemistry.** Formaldehyde- or paraformaldehyde-fixed tumor tissues were embedded in paraffin, and sections were stained with hematoxylin and eosin using standard techniques. Bromodeoxyuridine (BrdU) labeling was achieved by intraperitoneal injection of 1 mg/ml BrdU 30 minutes before sacrifice. eSZ cells were cultured on chamber slides and were fixed with 100% methanol. *EWS-FLI1* and *EWS-ERG* antigens were detected using a polyclonal rabbit anti-FLAG antibody (Sigma-Aldrich) in conjunction with the VECTOR M.O.M. Immunodetection Kit (Vector Laboratories) or FITC-conjugated anti-rabbit immunoglobulin. The following primary antibodies were used: anti-BrdU (Molecular

**Table 3**  
IC<sub>50</sub> values of inhibitors

Tumor cells	Inhibitors			
	iCRT14 (μM)	PNU74654 (μM)	DZNeP (μM)	Olaparib (μM)
mES #1	5.90	2.08	0.68	7.07
mES #5	5.61	6.79	10.30	2.36
mES #33	0.76	1.96	10.95	17.50
hES_EWS	1.71	2.98	13.46	0.86
hES_KH	7.41	6.05	15.87	2.70
hCGS_KAS	2.16	3.16	16.58	28.85
hOS_U2OS	14.79	3.42	19.33	40.42

Probes), anti-mouse CD99 (a gift of Dietmar Vestweber, Max Planck Institute for Molecular Biomedicine, Muenster, Germany), anti-COL2A (Millipore), anti-S100 (Dako), anti-COL10 (SLS), anti-CD57 (Sigma-Aldrich), anti-NGFR (Millipore), anti-β-catenin (Becton Dickinson), anti-nestin (Chemicon), and anti-myosin (Nihon). Immunofluorescent images were photographed with a Zeiss LSM 710 laser scanning microscope with a ×40 objective (Zeiss) and LSM Software ZEN 2009 (Zeiss).

**Western blotting.** Western blot analysis was performed using lysates of whole tumor tissues as described previously (54).

**RT-PCR and real-time quantitative RT-PCR.** Total RNA extraction, reverse transcription, and RNA quantification were performed according to methods described previously (54). Conventional RT-PCR and real-time quantitative RT-PCR were performed by using a Gene Amp 9700 thermal cycler (Applied Biosystems) and a 7500 Fast Real-Time PCR System (Applied Biosystems), respectively. The sequences of the oligonucleotide primers are shown in Supplemental Excel File 6.

**Luciferase assay.** A 1,340-bp genomic DNA fragment upstream from the murine *Gdf5* exon 1 was amplified by PCR using the following primers: forward (5'-TTCTATAATCCTACTCTGTAG-3') and reverse (5'-CTGAAAATAACTCGTTCTTG-3'). The fragment was inserted into the pGL4.10 vector (Promega) and transfected into eSZ, eGP, eSyR, or trunk cells using Lipofectamine 2000 (Invitrogen). Luciferase assays were performed as described previously (54).

**In vitro differentiation assay.** Cells were plated at 2 × 10<sup>5</sup> cells per well in 6-well plates and cultured in growth medium. Adipogenic, chondrogenic, osteogenic, myogenic, and neurogenic differentiation assays were conducted according to the methods previously described (55–57).

**Microarray analysis.** GeneChip analysis was conducted to determine gene expression profiles. A per cell normalization method was applied to eSZ and eGP samples (58). Briefly, cellular lysates were prepared with RLT buffer (QIAGEN). After RNA cocktails were added to the cell lysates according to the amount of DNA, total RNA was extracted using the RNeasy Mini Kit (QIAGEN). The murine Genome 430 2.0 Array (Affymetrix) was hybridized with aRNA probes generated from eSZ and eGP cells and murine Ewing's sarcoma tissue. After staining with streptavidin-phycoerythrin conjugates, arrays were scanned using an Affymetrix GeneChip Scanner 3000 and analyzed using Affymetrix GeneChip Command Console Software (Affymetrix) and GeneSpring GX 11.0.2 (Agilent Technologies) as described previously (59). The expression data for eSZ and eGP cells were converted to mRNA copy numbers per cell by the Percellome method, quality controlled, and analyzed using Percellome software (58). GSEA was performed using GSEA-P 2.0 software (60).

**Data comparisons and clustering between murine and human microarray data sets.** The microarray data from 10 murine Ewing's sarcoma samples were compared with human microarray data sets. Data from the ONCOMINE

database (<https://www.oncomine.org/>) were accessed in June 2011. Five microarray studies containing 117 tumor samples that were analyzed using Human Genome U133A Array (Affymetrix) were queried for gene expression. CEL files from E-MEXP-353 (61), E-MEXP-1142 (62), GSE6481 (63), GSE7529 (64), GSE21122 (65), GSE6461 (66), GSE42548 (67), GSE23972 (68), GSE20196 (69), and GSE10172 (70) were downloaded. The probe sets of the human U133A array were translated into 23,860 murine 430 2.0 arrays by the translation function of GeneSpring using Entrez Gene ID to make a novel common platform. Hierarchical clustering was achieved using log-transformed data and the following procedure. For the initial statistical

analysis, 13,026 genes that showed a “present” or “marginal” call in at least 24 of a total of 32 human Ewing's sarcoma samples were selected. Then, 12,340 probes were selected by 1-way ANOVA ( $P < 0.05$ ) analysis. Finally, 1,819 probes that showed >2-fold differences of expression in at least 3 tumor types were selected. With these 1,819 probes, hierarchical clustering was performed using the average linkage method and the Pearson's centered measurements. In addition, a probe set consisting of the 2,000 sequences that were the most altered in expression in human and mouse round cell tumors (Ewing's sarcoma, neuroblastoma, poorly differentiated synovial sarcoma, and malignant lymphoma) was used to distinguish each tumor from the other 3 using a fold-change analysis. Then, the frequencies of these 2,000 probes were compared between mouse Ewing's sarcoma and 4 human tumor types and between human Ewing's sarcoma and 4 mouse tumor types to find the closest tumor type using similar entities from GeneSpring.

**ChIP.** A total of 5 × 10<sup>6</sup> cells per immunoprecipitation were cross-linked with 10% formaldehyde for 10 minutes at room temperature. Histone immunoprecipitation was performed with anti-histone antibodies targeted against H3K9/K14Ac, H3K4/me3, H3K27/me3, total H3 (Cell Signaling Technologies), or H3K9/me3 (Millipore) pre-conjugated to protein G magnetic beads. Immunoprecipitated DNA was amplified with primers specific for each region. Sequences are shown in Supplemental Excel File 6.

**Cre/loxP-mediated gene silencing.** eSZ cells were transduced with a floxed *EWS-FLI1* retrovirus, and Ewing's sarcoma cells were obtained from a subcutaneous tumor developed in a nude mouse. Tumor cells were transduced with pMSCV-Cre-puro retrovirus in vitro. Senescence-associated β-galactosidase expression was detected using a Senescence Detection Kit (Biossion) 4 days after transduction of the retrovirus.

**siRNA interference studies.** For knockdown of *FLI1*, *Dkk2*, *Catnb*, *Prkcb1*, *Ezh2*, *Igfl*, *Dkk1*, and *Erg*, siRNAs were purchased from QIAGEN. The list of siRNAs is shown in Supplemental Excel File 7. siRNAs were introduced into mouse Ewing's sarcoma cells according to the manufacturer's protocol. Knockdown efficiencies were confirmed by Western blotting using anti-FLAG (Sigma-Aldrich), anti-ERG and anti-PKC β1 (Santa Cruz Biotechnology), anti-β-catenin (Becton Dickinson), and anti-EZH2 (Cell Signaling Technologies) or RT-PCR.

**Pharmacological experiments with specific inhibitors.** Mouse Ewing's sarcoma cells were treated with MEK1 inhibitor U0126 (Cell Signaling Technologies) in vitro. Both mouse and human Ewing's sarcoma cell lines were treated with WNT/β-catenin inhibitors, iCRT14 and PNU74654 (Tocris Bioscience); an EZH2 inhibitor, DZNeP (Cayman Chemical); or a PARP1 inhibitor, olaparib (Selleckchem), both in vitro and in vivo. Inhibition of ERG phosphorylation was examined by Western blotting using anti-P-ERK1/2 and anti-ERK1/2 (Cell Signaling



Technologies). For in vivo experiments,  $1 \times 10^6$  tumor cells were transplanted subcutaneously into nude mice, and the mice were treated with specific inhibitors when the tumor diameter reached 5 mm. All the inhibitors were dissolved in 0.2% DMSO, and they were administered by intraperitoneal injection 3 times per week.

**Cell cycle assay.** Single-cell suspensions were permeabilized with 0.1% Triton X-100 in PBS, and 50 mg/ml propidium iodide and 1 mg/ml RNase A were added. The cell suspensions were then analyzed by using a FACSCalibur flow cytometer and ModFit software (Becton Dickinson).

**Cloning retroviral integration sites.** Retroviral integration sites of individual mouse Ewing's sarcoma were isolated by inverse PCR, sequenced, and mapped as described previously (71).

**Accession numbers.** The microarray data sets are accessible through the NCBI Gene Expression Omnibus (GEO) database (<http://www.ncbi.nlm.nih.gov/geo>), with accession numbers GSE32615 and GSE32618.

**Statistics.** Continuous distributions were compared with 2-tailed Student's *t* test. Survival analysis was performed using the Kaplan-Meier life table method, and survival between groups was compared with the log-rank test. The 2-proportion *z* test was used to evaluate the significance of differences in the matched probe sets between 2 tumor types. All *P* values were 2 sided, and a *P* value of less than 0.05 was considered significant.

**Study approval.** Animals were handled in accordance with the guidelines of the animal care committee at the Japanese Foundation for Cancer Research, which gave ethical approval for these studies.

## Acknowledgments

We thank W. Kurihara and T. Kouji for helping with the microarray analyses; S.J. Baker (St Jude Children's Research Hospital, Memphis, Tennessee, USA) for EWS-FLI1 cDNA; and D. Vestweber (Max Planck Institute for Molecular Biomedicine, Muenster, Germany) for anti-mouse CD99. The research was funded by Grant-in-Aid for Scientific Research on Priority Areas Cancer 17013086 from Ministry of Education, Culture, Sports, Science and Technology and Grant-in-Aid for Young Scientists 23791672 from Japan Society for the Promotion of Science.

Received for publication July 29, 2013, and accepted in revised form April 10, 2014.

Address correspondence to: Takuro Nakamura, 3-8-31 Ariake, Koto-ku, Tokyo 135-8550, Japan. Phone: 81.3.3570.0462; Fax: 81.3.3570.0463; E-mail: takuro-ind@umin.net.

- Bernstein M, et al. Ewing's sarcoma family of tumors: current management. *Oncologist*. 2006;11(5):503–519.
- Ewing J. Diffuse endothelioma of bone. *Proc New York Pathol Soc*. 1921;21:17–24.
- Hu-Lieskovan S, Zhang J, Wu L, Shimada H, Schofield DE, Triche TJ. EWS-FLI1 fusion protein up-regulates critical genes in neural crest development and is responsible for the observed phenotype of Ewing's family of tumors. *Cancer Res*. 2005;65(11):4633–4644.
- Tirode F, Laud-Duval K, Prieur A, Delorme B, Cahrbord P, Delattre O. Mesenchymal stem cell features of Ewing tumors. *Cancer Cell*. 2007;11(5):421–429.
- Delattre O, et al. Gene fusion with an ETS DNA-binding domain caused by chromosome translocation in human tumours. *Nature*. 1992;359(6391):162–165.
- Zucman J, et al. Combinatorial generation of variable fusion proteins in the Ewing family of tumours. *EMBO J*. 1993;12(12):4481–4487.
- Sorensen PH, Lessnick SL, Lopez-Terrada D, Liu XF, Triche TJ, Denny CT. A second Ewing's sarcoma translocation, t(21;22), fuses the EWS gene to another ETS-family transcription factor, ERG. *Nat Genet*. 1994;6(2):146–151.
- Ordenez JL, Osuna D, Herrero D, de Alava E, Madoz-Gurpide J. Advances in Ewing's sarcoma research: where are we now and what lies ahead? *Cancer Res*. 2009;69(18):7140–7150.
- Riggi N, et al. Development of Ewing's sarcoma from primary bone marrow-derived mesenchymal progenitor cells. *Cancer Res*. 2005;65(24):11459–11468.
- Castillero-Trejo Y, Eliazar S, Xiang L, Richardson JA, Ilaria RL Jr. Expression of the EWS/FLI-1 oncogene in murine primary bone-derived cells results in EWS/FLI-1-dependent, Ewing sarcoma-like tumors. *Cancer Res*. 2005;65(19):8698–8705.
- Arndt CAS, Crist WM. Common musculoskeletal tumors of childhood and adolescence. *N Engl J Med*. 1999;341(5):342–352.
- Iwamoto M, et al. 2007. Transcription factor ERG and joint and articular cartilage formation during mouse limb and spine skeletogenesis. *Dev Biol*. 2007;305(1):40–51.
- Koyama E, et al. A distinct cohort of progenitor cells participates in synovial joint and articular cartilage formation during mouse limb skeletogenesis. *Dev Biol*. 2008;316(1):62–73.
- Mundy C, et al. Synovial joint formation requires local Ext1 expression and heparin sulfate production in developing mouse embryo limbs and spine. *Dev Biol*. 2011;351(1):70–81.
- Ambros IM, Ambros PF, Strehl S, Kovar H, Gadner H, Salzer-Kuntschik M. MIC2 is a specific marker for Ewing's sarcoma and peripheral primitive neuroectodermal tumors. Evidence for a common histogenesis of Ewing's sarcoma and peripheral primitive neuroectodermal tumors from MIC2 expression and specific chromosome aberration. *Cancer*. 1991;67(7):1886–1893.
- Bixel G, Kloep S, Butz S, Petri B, Engelhardt B, Vestweber D. Mouse CD99 participates in T-cell recruitment into inflamed skin. *Blood*. 2004;104(10):3205–3213.
- Vortkamp A, Lee K, Lanske B, Segre GV, Kronenberg HM, Tabin CJ. Regulation of rate of cartilage differentiation by Indian hedgehog and PTH-related protein. *Science*. 1996;273(5275):613–622.
- Sohaskey ML, Yu J, Diaz MA, Plaas AH, Harland RM. JAWS coordinates chondrogenesis and synovial joint positioning. *Development*. 2008;135(13):2215–2220.
- Vijayaraj P, et al. Erg is a crucial regulator of endocardial-mesenchymal transformation during cardiac valve morphogenesis. *Development*. 2012;139(21):3973–3985.
- Storm EE, Kingsley DM. GDF5 coordinates bone and joint formation during digit development. *Dev Biol*. 1999;209(1):11–27.
- St-Jacques B, Hammerschmidt M, McMahon AP. Indian hedgehog signaling regulates proliferation and differentiation of chondrocytes and is essential for bone formation. *Genes Dev*. 1999;13(16):2072–2086.
- Mak KK, Kronenberg HM, Chuang PT, Mackem S, Yang Y. Indian hedgehog signals independently of PTHrP to promote chondrocyte hypertrophy. *Development*. 2008;135(11):1947–1956.
- Toomey EC, Schiffman JD, Lessnick SL. Recent advances in the molecular pathogenesis of Ewing's sarcoma. *Oncogene*. 2010;29(32):4504–4516.
- James CG, Stanton LA, Agoston H, Ulici V, Underhill TM, Beier F. Genome-wide analyses of gene expression during mouse endochondral ossification. *PLoS One*. 2010;5(1):e8693.
- Honsei N, Ikuta T, Kawana K, Kaneko Y, Kawajiri K. Participation of nuclear localization signal 2 in the 3'-ETS domain of FLI1 in nuclear translocation of various chimeric EWS-FLI1 oncoproteins in Ewing tumor. *Int J Oncol*. 2006;29(3):689–693.
- Miyagawa Y, et al. EWS/ETS regulates the expression of the Dickkopf family in Ewing family tumor cells. *PLoS One*. 2009;4(2):e4634.
- Surdez D, et al. Targeting the EWSR1-FLI1 oncogene-induced protein kinase PKC- $\beta$  abolishes Ewing sarcoma growth. *Cancer Res*. 2012;72(17):4494–4503.
- Richter GH, et al. EZH2 is a mediator of EWS/FLI1 driven tumor growth and metastasis blocking endothelial and neuro-ectodermal differentiation. *Proc Natl Acad Sci U S A*. 2009;106(13):5324–5329.
- Nishimori H, et al. The Id2 gene is a novel target of transcriptional activation by EWS-ETS fusion proteins in Ewing family tumors. *Oncogene*. 2002;21(54):8302–8309.
- Smith R, et al. Expression profiling of EWS/FLI1 identifies NKX2.2 as a critical target gene in Ewing's sarcoma. *Cancer Cell*. 2006;9(5):405–416.
- Kinsey M, Smith R, Lessnick SL. NR0B1 is required for the oncogenic phenotype mediated by EWS/FLI1 in Ewing's sarcoma. *Mol Cancer Res*. 2006;4(11):851–859.
- Abaan OD, Levenson A, Khan O, Furth PA, Uren A, Toretsky JA. PTPL1 is a direct transcriptional target of EWS-FLI1 and modulates Ewing's sarcoma tumorigenesis. *Oncogene*. 2005;24(16):2715–2722.
- Wakahara K, et al. EWS-FlI1 up-regulates expression of the Aurora A and Aurora B kinases. *Mol Cancer Res*. 2008;6(12):1937–1945.
- Luo W, Gangwal K, Sankar S, Boucher KM, Thomas D, Lessnick SL. GSTM4 is a microsatellite-containing EWS/FLI target involved in Ewing's sarcoma oncogenesis and therapeutic resistance. *Oncogene*. 2009;28(46):4126–4132.
- Fuchs B, Inwards C, Scully SP, Janknecht R. hTERT is highly expressed in Ewing's sarcoma and activated by EWS-ETS oncoproteins. *Clin Orthop Relat Res*. 2004;426(426):64–68.
- Watanabe G, et al. Induction of tenascin-C by tumor-specific EWS-ETS fusion genes. *Genes Chromosomes Cancer*. 2003;36(3):224–232.
- Deneen B, Hamidi H, Denny CT. Functional analysis of the EWS/ETS target gene uridine phosphorylase. *Cancer Res*. 2003;63(14):4268–4274.
- Hahm KB, et al. Repression of the gene encoding the TGF-beta type II receptor is a major target of the EWS-FLI1 oncoprotein. *Nat Genet*. 1999;23(2):222–227.
- Dohjima T, Ohno T, Banno Y, Nozawa Y, Wen-yi Y, Shimizu K. Preferential down-regulation of phospholipase C-beta in Ewing's sarcoma cells transfected with antisense EWS-FlI-1. *Br J Cancer*. 2000;82(1):16–19.
- Scotlandi K, et al. Insulin-like growth factor I receptor-mediated circuit in Ewing's sarcoma/peripheral



- neuroectodermal tumor: a possible therapeutic target. *Cancer Res.* 1998;56(20):4570–4574.
41. Balamuth NJ, Womer RB. Ewing's sarcoma. *Lancet Oncol.* 2010;11(2):184–192.
  42. Niehrs C. Function and biological roles of the Dickkopf family of Wnt modulators. *Oncogene.* 2006;25(57):7469–7481.
  43. Mikheev AM, Mikheeva SA, Liu B, Cohen P, Zarbl H. A functional genomics approach for the identification of putative tumor suppressor genes: Dickkopf-1 as suppressor of HeLa cell transformation. *Carcinogenesis.* 2004;25(1):47–59.
  44. Uren A, Wolf V, Sun YF, Azari A, Rubin JS, Toretsky JA. Wnt/Frizzled signaling in Ewing sarcoma. *Pediatr Blood Cancer.* 2004;43(3):243–249.
  45. Garnett MJ, et al. Systematic identification of genomic markers of drug sensitivity in cancer cells. *Nature.* 2012;483(7391):570–575.
  46. Deneen B, Denny CT. Loss of p16 pathways stabilizes EWS/FLI1 expression and complements EWS/FLI1 mediated transformation. *Oncogene.* 2001;20(46):6731–6741.
  47. Sohn EJ, Li H, Reldy K, Beers LF, Christensen BL, Lee SB. EWS/FLI1 oncogene activates caspase 3 transcription and triggers apoptosis in vivo. *Cancer Res.* 2010;70(3):1154–1163.
  48. Riggi N, et al. EWS-FLI-1 modulates miRNA145 and SOX2 expression to initiate mesenchymal stem cell reprogramming toward Ewing sarcoma cancer stem cells. *Genes Dev.* 2010;24(9):916–932.
  49. Grier HE. The Ewing family of tumors: Ewing's sarcoma and primitive neuroectodermal tumors. *Pediatr Clin North Am.* 1997;44(4):991–1004.
  50. Soliman H, Ferrari A, Thomas D. Sarcoma in the young adult population: An international view. *Semin Oncol.* 2009;36(3):227–236.
  51. Martins AS, et al. A pivotal role for heat shock protein 90 in Ewing sarcoma resistance to anti-insulin-like growth factor 1 receptor treatment: in vitro and in vivo study. *Cancer Res.* 2008;68(15):6260–6270.
  52. Glade Bender JL, et al. Phase I pharmacokinetic and pharmacodynamics study of pazopanib in children with soft tissue sarcoma and other refractory solid tumors: a children's oncology group phase I consortium report. *J Clin Oncol.* 2013;31(24):3034–3043.
  53. Jin G, et al. Trib1 and Evi1 cooperate with Hoxa and Meis1 in myeloid leukemogenesis. *Blood.* 2007;109(9):3998–4005.
  54. Kawamura-Saito M, et al. Fusion between CIC and DUX4 up-regulates PEA3 family genes in Ewing-like sarcomas with t(4;19)(q35;q13) translocation. *Hum Mol Genet.* 2006;15(13):2125–2137.
  55. Pittenger MF, et al. Multilineage potential of adult human mesenchymal stem cells. *Science.* 1999;284(5411):143–147.
  56. Sakaguchi Y, Sekiya I, Yagishita K, Muneta T. Comparison of human stem cells derived from various mesenchymal tissues: superiority of synovium as a cell source. *Arthritis Rheum.* 2005;52(8):2521–2529.
  57. Shiota M, et al. Isolation and characterization of bone marrow-derived mesenchymal progenitor cells with myogenic and neuronal properties. *Exp Cell Res.* 2007;313(5):1008–1023.
  58. Kanno J, et al. "Per cell" normalization method for mRNA measurement by quantitative PCR and microarrays. *BMC Genomics.* 2006;7:64.
  59. Fujino T, et al. Function of EWS-POU5F1 in sarcomagenesis and tumor cell maintenance. *Am J Pathol.* 2010;176(4):1973–1982.
  60. Subramanian A, Kuehn H, Gould J, Tamayo P, Mesirov JP. GSEA-P: a desktop application for gene set enrichment analysis. *Bioinformatics.* 2007;23(23):3251–3253.
  61. Henderson SR, et al. A molecular map of mesenchymal tumors. *Genome Biol.* 2005;6(9):R76.
  62. Schaefer KL, et al. Microarray analysis of Ewing's sarcoma family of tumours reveals characteristic gene expression signatures associated with metastasis and resistance to chemotherapy. *Eur J Cancer.* 2008;44(5):699–709.
  63. Nakayama R, et al. Gene expression analysis of soft tissue sarcomas: characterization and reclassification of malignant fibrous histiocytoma. *Mod Pathol.* 2007;20(7):749–759.
  64. Albino D, et al. Identification of low intratumoral gene expression heterogeneity in neuroblastic tumors by genome-wide expression analysis and game theory. *Cancer.* 2008;113(6):1412–1422.
  65. Barretina J, et al. Subtype-specific genomic alterations define new targets for soft-tissue sarcoma therapy. *Nat Genet.* 2010;42(8):715–721.
  66. Haldar M, et al. A conditional mouse model of synovial sarcoma: insights into a myogenic origin. *Cancer Cell.* 2007;11(4):375–388.
  67. Teitz T, et al. Th-MYCN mice with caspase-8 deficiency develop advanced neuroblastoma with bone marrow metastasis. *Cancer Res.* 2013;73(13):4086–4097.
  68. Jeannot R, et al. Oncogenic activation of the Notch1 gene by deletion of its promoter in Ikaros-deficient T-ALL. *Blood.* 2010;115(25):5443–5454.
  69. Nakayama R, et al. Gene expression profiling of synovial sarcoma: distinct signature of poorly differentiated type. *Am J Surg Pathol.* 2010;34(11):1599–1607.
  70. Masque-Soler N, Szczepanowski M, Kohler CW, Spang R, Klapper W. Molecular classification of mature aggressive B-cell lymphoma using digital multiplexed gene expression on formalin-fixed paraffin-embedded biopsy specimens. *Blood.* 2013;122(11):1985–1986.
  71. Tanaka M, Jin G, Yamazaki Y, Takahara T, Takuwa M, Nakamura T. Identification of candidate cooperative genes of the Apc mutation in transformation of the colon epithelial cell by retroviral insertional mutagenesis. *Cancer Sci.* 2008;99(5):979–985.